Nuclear Instruments and Methods in Physics Research A 654 (2011) 522–526

Contents lists available at ScienceDirect

Nuclear Instruments and Methods in Physics Research A

journal homepage: www.elsevier.com/locate/nima

# Comparison of FANS and ARCS incoherent inelastic neutron scattering measurements of hydrogen trapped at dislocations in deformed Pd

Hyunsu Ju [a], Brent J. Heuser [a,*], Douglas L. Abernathy [b], Terrence J. Udovic [c]

[a] Department of Nuclear, Plasma, and Radiological Engineering, University of Illinois, Urbana, IL 61801, USA
[b] Neutron Scattering Sciences Division, Oak Ridge National Laboratory, Oak Ridge, TN 37831, USA
[c] NIST Center for Neutron Research, National Institute of Standards and Technology, Gaithersburg, MD 20899,USA

ARTICLE INFO

*Article history:*
Received 21 April 2011
Received in revised form
28 June 2011
Accepted 12 July 2011
Available online 22 July 2011

*Keywords:*
Hydrogen
Dislocation trapping
Inelastic neutron scattering
Vibrational density of states

ABSTRACT

Incoherent inelastic neutron scattering (IINS) measurements of the vibrational density of states (VDOS) of hydrogen trapped at dislocations in deformed $PdH_{0.0013}$ have been performed using ARCS at the SNS and FANS at the NCNR. A comparison of data sets at 4 and 295 K indicates good agreement of the measured VDOS for the two instruments. The low hydrogen inventory ($\sim 10^{-3}$ g) provides a test of the response of each instrument over the energy transfer range of 40–100 meV corresponding to the vibrational density of states of the hydrogen modes.

© 2011 Elsevier B.V. All rights reserved.

## 1. Introduction

Incoherent inelastic neutron scattering (IINS) has found wide utility in the study of hydrogen in various crystalline materials [1–5]. Generally, the measured spectra after proper scaling are proportional to the vibrational density of states (VDOS). The VDOS represents normalized phonon density of states, quantifying the number of phonon modes or states per unit energy. For the Pd hydride, optic modes are typically assumed to be due solely to hydrogen since Pd has a single atom in the primitive cell and displacements are inversely proportional to mass. In the strictest sense, however, Pd displacements will couple to optic mode propagation, leading to a coherent (Pd has a very small incoherent scattering cross-section) inelastic intensity contribution. We have recently measured the VDOS of hydrogen trapped at dislocations in deformed polycrystalline $PdH_{0.0008}$ using the Filter-Analyzer Neutron Spectrometer (FANS) at 4 and 295 K [6]. These data support the hypothesis that trapped hydrogen undergoes a solid solution-to-hydride ($\alpha \rightarrow \beta$ or $\alpha \rightarrow \alpha'$) phase transformation upon cooling from 295 to 4 K. As demonstrated previously [6] and shown below in additional spectra, a shift of the primary peak energy from ~68 meV (corresponding to the local mode of dilute hydrogen in regular octahedral sites in α-Pd [7–9]) to ~58 meV (corresponding to the transverse optic phonon mode of β– or α′–Pd [10–12]) characterizes the response of the system upon cooling. This energy shift, together with significant peak broadening and peak asymmetry at 4 K [6], was the basis of the phase transformation hypothesis. This hypothesis has recently been supported by small-angle neutron scattering measurements of hydrogen segregation at dislocations in deformed single crystal Pd consistent with hydride phase formation at low temperature [13].

In this paper we present additional VDOS measurements using FANS and the Wide Angular-Range Chopper Spectrometer (ARCS) at the SNS [15] in the same sample matrix (deformed polycrystalline Pd with-hydrogen concentration $\sim 10^{-3}$ [H]/[Pd]) with-hydrogen inventories of ~1–2 mg at 4 and 295 K. The purpose of measuring the same sample matrix with two different instruments is two-fold. First, a comparison of the measured spectra will demonstrate that the VDOS is independent of spectroscopy method and data reduction, as expected. Second, the data sets facilitate a comparison of counting statistics for each instrument, and therefore spectroscopy method and neutron source.

Incoherent inelastic neutron scattering spectra are integrated over a large solid angle and corresponding wavevector transfer range $\Delta Q$. The IINS technique requires some form of energy discrimination to resolve neutron energy transfer, $E$. FANS resolves energy transfer by fixing the final energy with the Be–Bi–graphite composite filter (~1.2 meV average final energy with a ~1.1 meV full-width half-maximum resolution) and scanning the incident energy via a $\theta$–$2\theta$ rotation of a crystal monochromator-sample table assembly [14]. FANS operates on the 20 MW reactor at the NIST Center for Neutron Research. The FANS filter-detector array covers a solid angle range of $\Delta\Omega \sim 4\pi/10$ sr. The integrated

* Corresponding author. Tel.: +217 333 9610; fax: +217 333 2910.
*E-mail address:* bheuser@illinois.edu (B.J. Heuser).

0168-9002/$ - see front matter © 2011 Elsevier B.V. All rights reserved.
doi:10.1016/j.nima.2011.07.020

wavevector transfer range varies from $4 \le Q \le 5$ Å$^{-1}$ at $E_i = 40$ meV to $6 \le Q \le 7.5$ Å$^{-1}$ at $E = 100$ meV. For the current measurements, the energy transfer resolution varied over these limits from $\Delta E \sim 2$ to 5 meV, respectively. We note the resolution of the FANS instrument can be improved at lower incident intensity by adjusting the monochromator resolution. ARCS, on the other hand, is a chopper instrument operating on the 1.1 MW Spallation Neutron Source, a pulsed time-of-flight (TOF) facility. ARCS uses a Fermi chopper to fix the incident energy and total neutron TOF to determine final energy. The ARCS detector array covers a solid angle of $\Delta\Omega \sim 4\pi/5$ sr and a corresponding wavevector transfer range of $5 \le Q \le 12$ Å$^{-1}$ at an incident energy of $E_i = 150$ meV and $E$ from $\sim 0$ to 100 meV. This $Q$ range is applicable to the integrated VDOS data presented here. The full $Q$ range is larger: at the elastic line ($E \sim 0$) $0.5 \le Q \le 16$ Å$^{-1}$, at $E \sim 40$ meV $1 \le Q \le 15$ Å$^{-1}$, and at $E \sim 100$ meV $4 \le Q \le 13$ Å$^{-1}$. The energy resolution improves with $E$, varying from $\Delta E \sim 5$ to 2 meV over an energy transfer range of $E \sim 40$–100 meV, respectively. ARCS uses position sensitive detectors and can therefore provide $Q$–$E$ information without $\Delta Q$ integration.

Neutron scattering instruments on each type of source have advantages and disadvantages. Spallation sources are undermoderated with respect to the neutron spectrum exiting thermal and cold moderators. This leads to lower time-averaged on-sample neutron intensity in the sub-eV energy range compared to reactor sources. However, pulsed source-based instruments typically operate in the time domain and can therefore use neutron TOF information to record a wide range of $Q$ or $E$ in each pulse, compensating for reduced differential intensity. Another consideration is the operation of reactor-based filter-analyzer incoherent inelastic scattering instruments. Scanning incident energy permits efficient use of beam time since the user can select the energy transfer range of interest. In our measurements using FANS, for example, we scanned the range from $\sim 35$ to 105 meV exclusively, thereby devoting all measurement time to the hydrogen vibrational mode region. Chopper spectrometers, on the other hand, yield spectra over a large $Q$–$E$ space by default. While this is generally advantageous, it can represent additional information not of interest to the user. A comparison of $Q$–$E$ space for the FANS and ARCS instruments is shown in Fig. 1. The utility of a chopper spectrometer, especially the large covered $Q$ range, is evident. The statement related to this extensive parameter space provided by default is placed in proper context with this figure; the advantage of the TOF methodology is offset to a degree, at least for VDOS measurements, by the portions of unusable $Q$–$E$ space.

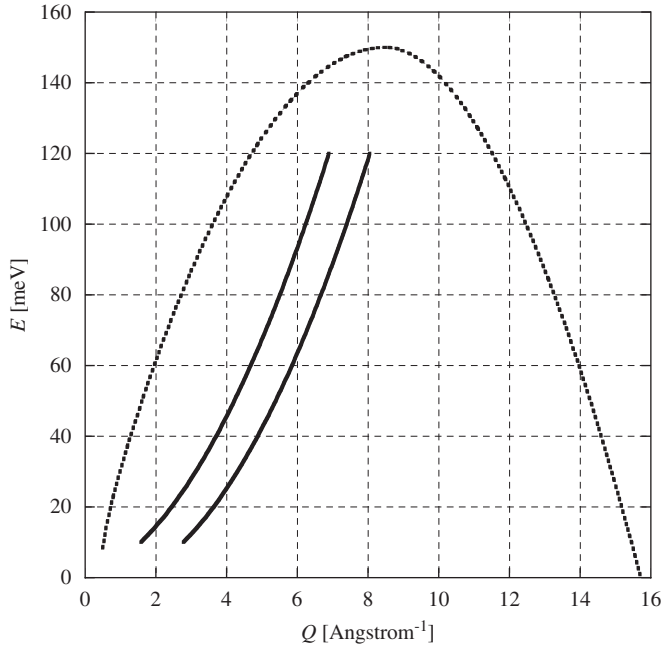


**Fig. 1.** Neutron energy transfer ($E$) versus wavevector transfer ($Q$) for ARCS (dotted line) and FANS (solid lines). Both boundaries in $E$–$Q$ space represent detector extremes ($\sim$3–135° for ARCS; $\sim$10–120° for FANS) and correspond to a fixed incident energy of $E_i = 150$ meV for ARCS and a fixed final energy of $E' = 1.2$ meV for FANS.

Experimental details are described in the next section. This includes a tabulation of sample and instrument properties and parameters. The IINS measurements at 4 and 295 K from each instrument are then presented and compared. Discussion will focus on overall similarity of the spectra from each instrument at a given temperature and a qualitative comparison of instrument performance.

## 2. Materials and methods

The polycrystalline Pd sample material used here was identical to that of Ref. [6]. Cold-rolled polycrystalline Pd sheet was supplied by Alpha Aesar with a purity of 99.98% (metal basis) and thickness of 0.25 mm. A cellular dislocation substructure is typical in cold-worked Pd, as observed with transmission electron microscopy [13]. The as-received sheet was cut into 0.3 × 5 cm pieces and subsequently cycled twice across the hydride miscibility gap by *ex situ* exposure to $H_2$ gas at ambient temperature. Hydride cycling is known to generate a relatively uniform dislocation substructure [13,16]. The cold-rolled, cycled polycrystalline material is referred to as the deformed Pd sample here. The FANS and ARCS IINS measurements were performed with the deformed sample held in an Al can mounted on a top-loading He closed cycle refrigerator (CCR). The total sample mass was increased from 21 g (Ref. [6]) to 103 g (current FANS measurement) and to 175 g (current ARCS measurement). The difference in sample mass between the two current measurements was due to the on-sample beam widths used, 2.5 versus 5 cm for FANS and ARCS, respectively. The FANS instrument can employ a 5 cm beam, but this option is no longer necessary with the larger composite filter now in use. The total hydrogen concentrations were 0.00130 and 0.00134 [H]/[Pd] for the FANS and ARCS measurements, respectively. These concentrations were measured directly by total $H_2$ gas pressure reduction in a Sievert's apparatus with a volume of approximately 2 l. Thus, the total hydrogen inventory was increased from 0.16 mg (Ref. [6]) to 1.3 and 2.2 mg for the current FANS and ARCS measurements, respectively.

The with-hydrogen deformed sample in each case was equilibrated *ex situ* with respect to hydrogen absorption at room temperature in the Al measurement can and then isolated with an all-metal valve. The Al can was then mounted to the CCR cold finger and inserted into the CCR sample well. The sample well was evacuated, backfilled with He exchange gas, and cooled to 4 K for the first IINS measurement on both instruments. On ARCS, the isolated sample was then heated to 295 K and re-measured, maintaining equilibrium with respect to $H_2$. On FANS, the isolated sample was incrementally heated and re-measured at 100, 200, and 295 K while maintaining equilibrium with respect to $H_2$. Here we present only the 4 and 294 K FANS spectra; the complete temperature series has recently been published by Trinkle et al. [17]. Generally, heating to 295 K results in a $\beta \rightarrow \alpha$ or $\alpha' \rightarrow \alpha$ phase transformation; IINS measurements in Ref. [6] and presented below to support this statement. A zero hydrogen concentration deformed reference sample was measured on each instrument at

**Table 1**
Sample and instrument parameters.

| Sample | $T$ [K] | Sample mass [g] | Hydrogen mass, $m_H$ [mg] | Meas. time, $\Delta t$ [h] | $\Delta\Omega$ [st] | $E_i$ [meV] | $E'$ [meV] |
|---|---|---|---|---|---|---|---|
| ARCS | | | | | 2.5 | 150 | 0–150 |
| $PdH_{0.00134}$ | 4 | 175 | 2.2 | 16 | | | |
| $PdH_{0.00134}$ | 295 | 175 | 2.2 | 16 | | | |
| Pd reference | 4 | 175 | 0 | 16 | | | |
| Pd reference | 295 | 175 | 0 | 12 | | | |
| FANS | | | | | 1.3 | 35–105 | 1.2 |
| $PdH_{0.00130}$ | 4 | 103 | 1.3 | 33 | | | |
| $PdH_{0.00130}$ | 295 | 103 | 1.3 | 33 | | | |
| Pd reference | 4 | 103 | 0 | 33 | | | |
| Pd reference | 295 | 103 | 0 | 33 | | | |
| $PdH_{0.63}$[†] | 4 | 21 | 124 | 0.17 | | | |
| $PdH_{0.015}$[†] | 295 | 21 | 3.0 | 4.3 | | | |
| $PdH_{0.0008}$[†] | 4 | 21 | 0.16 | 83 | | | |
| $PdH_{0.0008}$[†] | 294 | 21 | 0.16 | 122 | | | |

[†] From Ref. [6]. The measurement time for the deformed $PdH_{0.0008}$ sample at 4 and 295 K includes the zero hydrogen Pd background runs.

4 and 295 K by *ex situ* outgassing of the with-hydrogen sample for ~48 h at 120 °C under vacuum without removing the sample from the Al measurement can. The FANS fast neutron background was measured with the deformed sample in place by scanning incident energy with the detector bank blocked with 0.6 mm Cd sheet. All FANS spectra were normalized by total beam monitor count on a point-by-point basis. Normalization by total beam monitor eliminates the influence of minor reactor power fluctuations and correctly scales the data with respect to the $k'/k$ ratio, as described below. All ARCS spectra were normalized to total integrated on-target current (again to eliminate the influence of source power fluctuations), corrected for pixel sensitivity and pixel solid angle.

In addition to the deformed $PdH_{0.0013}$ 4 and 295 K measurements just described, a 4 K $PdH_{0.63}$ measurement and a 295 K measurement of well-annealed $PdH_{0.015}$ were previously measured with FANS [6] and are included here. Ref. [6] should be consulted for further details regarding these measurements. Relevant sample characteristics, measurement characteristics, and instrument properties are listed in Table 1.

## 3. Theory

The one-phonon emission (i.e., neutron down scattering employed for both FANS and ARCS measurements) incoherent inelastic scattering cross-section, per unit solid angle $\Omega$, per unit energy $E'$, is given by [18–20]

$$\frac{d^2\sigma}{d\Omega dE'} = \frac{\sigma_{inc}}{4\pi}\frac{k'}{k}\frac{N}{2M}\frac{Q^2}{\omega}[n(\omega)+1]e^{-2W}Z(\omega) \quad (1)$$

where $\sigma_{inc}$ is the incoherent microscopic cross-section, $M$ is the atomic mass, $N$ is the atoms per unit cell, $k'$ and $k$ are the scattered and incident wavevectors, respectively, $E'$ is the energy of the scattered neutron, $Q$ is the wavevector transfer, $\omega$ is the frequency of the phonon normal mode given by $\omega=(E_i\text{-}E')/\hbar=E/\hbar$, $n(\omega)$ is the Bose occupation factor given by $n(\omega)=\exp(-\hbar\omega/kT)$, $\exp(-2W)$ is the Debye–Waller factor with $2W=Q^2\langle u_d^2\rangle/3$ where $u_d$ is the atomic displacement and $\langle u_d^2\rangle$ is the mean value average of over the atoms in the unit cell [18], and $Z(\omega)$ is the normalized phonon density of states. For high incident energy $E_i$, $k'\ll k$ and $Q^2$ is proportional to $\omega$. Further, if $kT\ll\hbar\omega$, then $n(\omega)+1\sim1$ and the Debye–Waller factor slowly varies with $Q$. Under these assumptions, FANS spectra are proportional to the $Z(\omega)$, provided the spectra are recorded for constant monitor counts on a point-by-point basis. This requirement corrects for the $k'/k$ scaling in Eq. (1) when the monitor is a $1/v$ neutron absorber [19]. Time-of-flight IINS spectra are recorded in the time domain over an extended dynamic range, and thus cannot be normalized on a point-by-point basis using a beam monitor. For ARCS, these data are collected as discrete neutron events (discrete detector pixel and time-of-flight values) and converted directly into final neutron energy bins $dE'$. This conversion is represented by the Jacobian transformation $dE'/dt'\propto(t')^3$, where $t'$ is the time-of-flight from the sample to a given detector pixel. The binned data are scaled by the energy bin width, detector pixel solid angle and detector pixel sensitivity to provide a signal proportional to the double differential cross-section given by Eq. (1). Following Eq. (1), the binned data are then scaled by $k/k'$, $E/Q^2$, the Bose factor, and the Debye–Waller factor to yield a response proportional to $Z(w)$. Note that the $\sigma_{inc}/M$ ratio in Eq. (1) defines the incoherent response from the individual components of the system. In the case of the Pd–H system, the response is dominated by hydrogen ($\sigma_{inc}\sim80$ barns) and this response is largely, although not completely, incoherent. We assume here that the measured spectra (corrected and normalized intensity versus $E$) over an energy transfer range of ~40–100 meV represent the incoherent-averaged, one-phonon emission (neutron down scattering) VDOS from hydrogen.

## 4. Results

The foreground, background, and net spectra at 4 K from deformed $PdH_{0.0013}$ measured with ARCS and FANS are shown in Figs. 2 and 3, respectively. These data are normalized over the 35–40 meV energy transfer region where the Pd acoustic mode intensity dominates the response. An additional background subtraction from the net response has been performed, as shown

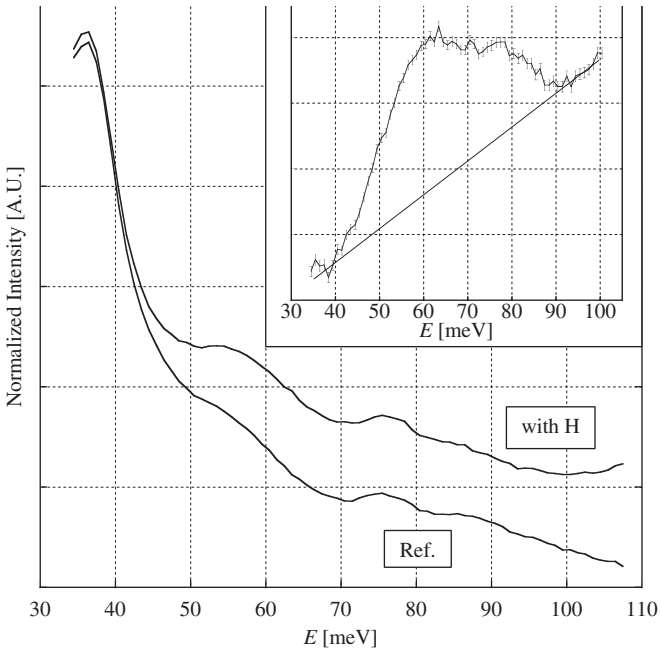


**Fig. 2.** Normalized ARCS spectra at 4 K with and without (Ref.) hydrogen as a function of neutron energy loss. Inset shows the net response (the reference spectrum subtracted from the with-hydrogen spectrum) and the linear background subtraction that accounts for additional contributions including multi-phonon events.

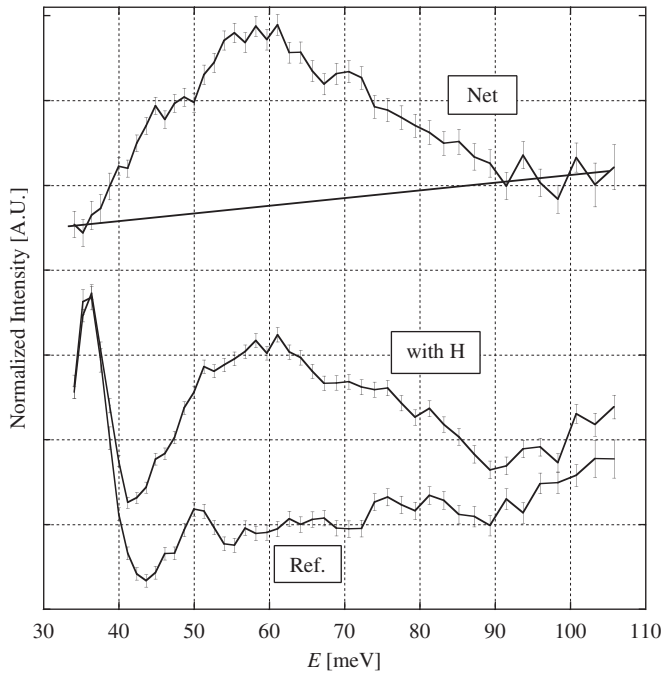


**Fig. 3.** Normalized FANS spectra at 4 K with and without (Ref.) hydrogen as a function of neutron energy loss. The net response (the reference spectrum subtracted from the with-hydrogen spectrum) is shown as well. The linear background subtraction that accounts for additional contributions including multi-phonon events is largely independent of neutron energy loss.

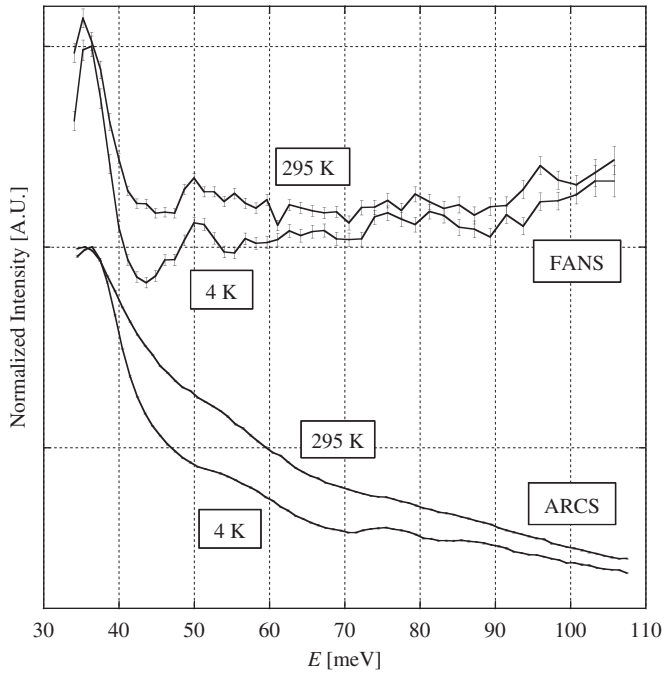


**Fig. 4.** FANS (the top set of curves) and ARCS (the bottom set of curves) background spectra at 4 and 295 K as a function of neutron energy loss. The background spectra were measured after each deformed polycrystalline Pd sample was outgassed to remove hydrogen, as described in the text. The background measurements for each set were normalized to the respective with-hydrogen measurement at each temperature for each instrument.

in each figure. This subtraction accounts for multiple phonon events and is highly energy-dependent in the case of the ARCS spectra. This is not a trivial situation and represents background sources and/or instrumental responses for ARCS that are currently not understood. In the FANS subtracted data, the spurious intensity [14] is eliminated by subtraction, rendering a relatively flat background beneath the hydrogen VDOS intensity. The background responses (the deformed Pd sample without hydrogen) at 4 and 295 K are compared in Fig. 4 for both instruments. These data have been normalized to the respective with-hydrogen measurements at each temperature for each instrument, as shown, for example, in Figs. 2 and 3 at 4 K. Both ARCS and FANS Pd background responses contain weak spurious scattering. The FANS spurious intensity is attributed to inelastic scattering events in Be (comprising of the composite filter) of elastically scattered neutrons from the sample [6,14]. The presence of Bi in the current FANS filter attenuates these spurious peaks by two orders of magnitude [14]. These features are somewhat sample dependent *via* the coherent response (Bragg diffraction) of the scattering system. The ARCS background exhibits broad features at ~55, ~75, and ~88 meV. These features may be sample dependent *via* the coherent response (Bragg diffraction) of the scattering system inducing inelastic scattering events with surrounding materials such as steel structure components. The net normalized spectra at 4 and 295 K from both instruments are compared in Fig. 5. Also included in this comparison are the 4 K $PdH_{0.63}$ and well-annealed 295 K $PdH_{0.015}$ spectra measured previously by FANS [6]. The normalization implemented in Fig. 5 yielded a peak intensity value of approximately 1 (hence, the use of arbitrary units) to

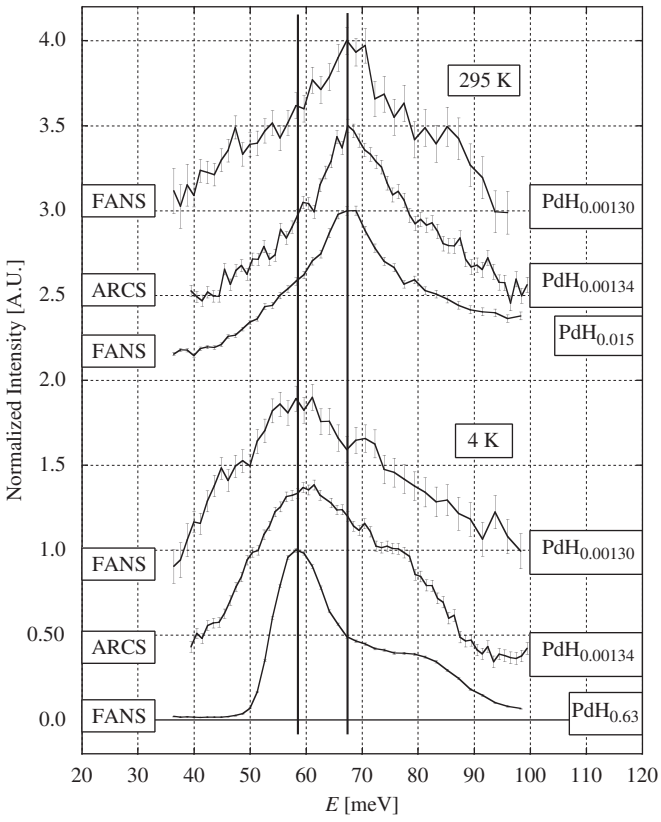


**Fig. 5.** Comparison of all FANS and ARCS spectra at 4 and 295 K. Solid vertical lines are drawn through the primary peaks of the $PdH_{0.63}$ ($E$~58 meV) and of the well-annealed $PdH_{0.015}$ ($E$~67 meV) spectra. Generally, the deformed 4 K $PdH_{0.0013}$ spectra recorded with both instruments exhibit a central peak at $E$~58 meV and a high-energy shoulder, corresponding to the TO mode (which lacks significant dispersion) and the LO mode (which does have significant dispersion), respectively. The broadening of the primary peak observed in deformed $PdH_{0.0013}$ at 4 K is attributed to a loss of degeneracy of the trapped hydrogen induced by local strain. The primary peak energy observed with each instrument from deformed $PdH_{0.0013}$ at 295 K is in agreement with the location of the local mode from well-annealed $PdH_{0.015}$.

facilitate a comparison of peak locations (on the energy axis) when the spectra are offset vertically.

## 5. Discussion

The spectra measured with FANS and ARCS from deformed $PdH_{0.0013}$ at 4 and 295 K agree, indicating both instruments and associated data reduction provide consistent quantification of the hydrogen VDOS. The central peak ($E\sim58$ meV) in the 4 K ARCS spectrum is slightly harder, while the opposite appears to hold at 295 K. The comparison of both sets of spectra with those measured from $PdH_{0.6}$ at 4 K and well-annealed $PdH_{0.015}$ at 295 K is consistent with the hydride to solid solution phase transformation at dislocations, as previously discussed in Ref. [6]. The significant peak broadening and high-energy shoulder observed previously at 4 K are again observed in the spectra from both instruments. As discussed in Ref. [6], these features are attributed to a loss of degeneracy of trapped hydrogen and dispersion on the longitudinal optic [LO] mode of the hydride phase [21], respectively. The loss of degeneracy is due to the local strain dislocation trapping environment perturbing the three-fold symmetry of the regular interstitial octahedral site, as confirmed by recent first principles calculations [17,22].

The point-by-point comparison of counting statistics of the $PdH_{0.0013}$ samples indicates improved performance for ARCS. The hydrogen inventory measured with ARCS was approximately a factor of two larger than that measured with FANS. Furthermore, the solid angle subtended with ARCS is a factor of two larger than that of FANS. Both factors favor improved counting statistics for ARCS, roughly by a factor of two because of the square-root dependence of the measured foreground intensity on these factors. However, the argument can be made that detector solid angle coverage is an inherent property of instrument performance. In this case, the correction for hydrogen inventory alone would favor ARCS by a factor of 1.4. The ARCS counting statistics appear to be better than this approximate factor, indicating the inherent performance of this instrument is greater than FANS. However, undefined background contributions exist with this instrument that must ultimately be understood and resolved. In particular, an additional energy-dependent background subtraction (Fig. 2 inset) is required for ARCS data. This issue must be considered in the comparison of counting statistics. On the other hand, the origin of background intensity is well understood for the FANS instrument [14]. This is not too surprising given the longer operating experience for this instrument. Moreover, it should be noted that FANS is being upgraded with a new monochromator system that will yield a factor of four in on-sample intensity and a second detector bank that will double the solid angle. The FANS upgrade will effectively increase the detector signal eightfold, thereby significantly enhancing performance.

The comparison of FANS and ACRS data from similar deformed sample matrices presented here represents a test of the ability of each instrument to characterize the vibrational density of states of trapped hydrogen at very low total hydrogen inventory ($\sim$1–2 mg). The overall agreement of the VDOS spectra obtained with a reactor-based and TOF-based instrument for this challenging problem may serve as a benchmark for the newer ARCS instrument.

## Acknowledgements

This work was supported by the NSF under Grant number DMR-0804810. In addition, we acknowledge the support of the National Institute of Standards and Technology, U.S. Department of Commerce, in providing the neutron research facilities used in this work. A portion of this research was performed at the Oak Ridge National Laboratory's Spallation Neutron Source and was sponsored by the Scientific User Facilities Division, Office of Basic Energy Sciences, U.S. Department of Energy.

## References

[1] M.R. Chowdhury, D.K. Ross, Solid State Commun 13 (1973) 229.
[2] A. Magerl, J.J. Rush, J.M. Rowe, D. Richter, H. Wipf, Phys. Rev. B 27 (1983) 927.
[3] J.J. Rush, J.M. Rowe, D. Richter, Phys. Rev. B 31 (1985) 6102.
[4] D.K. Ross, V.E. Antonov, E.L. Bokhenkov, A.I. Kolesnikov, Phys. Rev. B 58 (1998) 2591.
[5] J.J. Rush, T.J. Udovic, N.F. Berk, D. Richter, A. Magerl, Europhys. Lett. 48 (1999) 187.
[6] B.J. Heuser, T.J. Udovic, H. Ju, Phys. Rev. B 78 (2008) 214101.
[7] W. Drexel, A. Murani, D. Tocchetti, W. Kley, I. Sosnowska, D.K. Ross, J. Phys. Chem. Solids 37 (1976) 1135.
[8] J.J. Rush, J.M. Rowe, D. Richter, Z. Phys. B-Condens. Matter 55 (1984) 283.
[9] R. Kirchheim, X.Y. Huang, H.-D. Carstanjen, J.J. Rush, in: R.M. Latanision, R.H. Jones (Eds.), Chemistry and Physics of Fracture, Martinus Nijhoff Publishers, 1987, p. 580.
[10] J.M. Rowe, J.J. Rush, H.G. Smith, Phys. Rev. B 8 (1973) 6013.
[11] D.G. Hunt, D.K. Ross, J. Less-Common Met. 49 (1976) 169.
[12] A.I. Kolesnikov, I. Naatkaniec, V.E. Antonov, I.T. Belash, V.K. Fedotov, J. Krawczyk, et al., Physica B 174 (1991) 257.
[13] B.J. Heuser, H. Ju, Phys. Rev. B 83 (2011) 094103.
[14] T.J. Udovic, D.A. Neumann, J. Leão., C.M. Brown, Nucl. Instr. and Meth. Phys. Res. A 517 (2004) 189.
[15] D.L. Abernathy, Notiziario Neutroni e Luce di Sincrotrone 13 (2008) 4.
[16] B.J. Heuser, J.S. King, Met. Mat. Trans. A 29 (1998) 1593.
[17] D.R. Trinkle, H. Ju, B.J. Heuser, T.J. Udovic, Phys. Rev. B 83 (2011) 174116.
[18] G.L. Squires, Introduction to the Theory of Thermal Neutron Scattering, Cambridge University Press, Chambride, 1978.
[19] J.R.D. Copley, D.A. Neumann, W.A. Kamitakahara, Can. J. Phys. 73 (1995) 763.
[20] C.G. Windsor, Pulsed Neutron Scattering, Taylor and Frances, LTD, London, 1981.
[21] J.M. Rowe, J.J. Rush, H.G. Smith, M. Mostoller, H.E. Flotow, Phys. Rev. Lett. 33 (1974) 1297.
[22] H.M. Lawler, D.R. Trinkle, Phys. Rev. B 82 (2010) 172101.